Springer

KSME

Journal of Mechanical Science and Technology 24 (6) (2010) 1319~1327
www.springerlink.com/content/1738-494x
DOI 10.1007/s12206-010-0329-0

An accurate and simple model for flexible satellites for three-dimensional studies †

Shahram Shahriari[1,*], Shahram Azadi[2] and Majid M. Moghaddam[3]

[1]*Department of Mechanical Engineering, Tarbiat Modares University, Tehran, Iran*
[2]*Faculty of Mechanical Engineering, K. N. Toosi University of Technology, Tehran, Iran*
[3]*Faculty of Mechanical Engineering, Tarbiat Modares University, Tehran, Iran*

(Manuscript Received August 20, 2009; Revised March 16, 2010; Accepted March 16, 2010)

Abstract

In this paper, an accurate and simple model of a satellite with two flexible solar panels for three-dimensional dynamic studies is proposed and compared with other models. In the proposed model, each solar panel is assumed to be rigid and attached to the satellite body via a simple hinge, a torsional spring, and a torsional damper. Kane's method is utilized to derive the equations of motion. The model of flexible satellite with the assumption of Euler-Bernoulli beam for the solar panels, generally used in the literature, has been introduced for comparison. A comprehensive model of flexible satellite, considering solar panels as flexible and finite element panels, has been provided in ADAMS environment as a reference when comparing the two mentioned models. The Euler-Bernoulli model does not appropriately simulate the three-dimensional motion of satellite. Conversely, the hinged, rigid-panel model proposed in this paper provides suitable results in both two- and three-dimensional maneuvers.

Keywords: Satellite; Dynamic modeling; Flexibility; Kane's method; Solar panels

1. Introduction

Modern satellites need a huge amount of electrical energy to trigger different equipment. The solar panels attached to the satellites can be used to perform such an activity. However, the structure of solar panels usually limits their capability to absorb sunlight. To increase absorption of solar energy, solar panels are designed with expanded surfaces. On the other hand, to reduce the weight of panels, thin structures that amplify the flexibility of solar panels are used.

The rotation and attitude compensation of a satellite cause some vibrations, which have a negative effect on satellite attitude, in the solar panels. This is the main reason why many researchers focused their work on the identification and attitude control of satellites with flexible panels.

To design the attitude control system of a satellite, an appropriate model for the satellite is necessary. The satellite model should be simple yet capable of accurately simulating the actual movement of the system. The behavior of a fairly complete model of a flexible satellite in ADAMS is similar to that of a real satellite since it includes all possible mode shapes of flexible panels. To use the controller-design facilities of MATLAB, the designer should build an appropriate and simple satellite model from this software. The ADAMS model can then be used as a virtual or laboratory system for utilizing the designed controller and simulating its function on a real satellite. In addition, the ADAMS model can be used as a base for validating and determining the accuracy of a simplified model in MATLAB.

Researchers [1-6] have limited their work in the planar motion of a satellite and its rotation about the normal axis of the motion plane. Planar motion study helps overcome most of the challenges in modeling three-dimensional motions, facilitates the use of accurate and simple models, such as the Euler-Bernoulli beam, and exerts mode summation procedure. The planar model and mode summation procedure have been used to model flexible satellite utilizing adaptive control [1] and control design based on the lyapunov stability theory [2].

In [3], the effect of using the active control method to reduce vibration in the planar motion via a piezoelectric is determined by using the Euler-Bernoulli model. In addition, vibration control on a planar model is presented in [4]. For simulating the vibration of solar panels, the mode summation procedure is used in this reference. The required dynamic model can be produced via examinations on a real satellite or laboratory setup [5-7].

† This paper was recommended for publication in revised form by Associate Editor Eung-Soo Shin

*Corresponding author. Tel.: +98 9122006848, Fax: +98 44196796
E-mail address: shahriari2000@gmail.com

© KSME & Springer 2010

In [5], the attitude control of a satellite with an L-shaped flexible appendage was done experimentally on a laboratory setup. The motion was planar, and an L-shaped appendage is located in the plane of motion. The natural frequencies of the system are measured for experiment purposes, and the transfer function of the system is determined based on these frequencies and is used in controller design. The vibration of the flexible appendage is controlled by attaching infrared sensors and a piezoceramic actuator to the L-shaped flexible appendage of the above-mentioned laboratory setup [6]. Since the attitude change of many of the satellites and all of the spacecrafts is three dimensional, the assumption of planar motion and the use of the Euler-Bernoulli beam do not simulate the real behavior of the system.

In [7], the required modeling for the three-dimensional controller design of a satellite equipped with a pair of huge flexible solar panels is done using some testing on a real satellite while the satellite is moving on an orbit. The transfer function between the input torque to the body and body angle is obtained for each of the three directions of the coordinate axes of the satellite. The transfer function is considered in the form of summation of the transfer function of the rigid body and the transfer function of a number of vibration modes for each direction. To determine related parameters, the input torque takes the form of a quasi-random signal in tests, and the least-squares method is used.

Some researchers have studied the three-dimensional motion of a satellite and have simulated flexible panels in the form of the Euler-Bernoulli model. [8-10]

In [8], the equations of the three-dimensional motion of a satellite are obtained, aiding the Lagrange method, using just one mode and ignoring torsion and in-plane bending of panels. In [9], the mode summation procedure is used to simulate solar panels, and 12 bending modes have been taken into account, thereby improving the simulation. However, torsion modes have been ignored. Some torsion modes are exist between the first and twelfth bending modes, considering twelve bending modes while a number of torsion modes have been ignored, are not essential and slow down numerical calculations. Utilizing the Euler equation, the equations of a satellite in three-dimensional motion as well as the Euler-Bernoulli beam for solar panels are derived in [10]. Considering the panel model in the three-dimensional motions of a satellitesatellite as aan Euler-Bernoulli beam causes disregard of the gyroscopic effect of panels and increases the error in the results.

For creating an analytical model of a satellite with flexible solar panels, the finite element method is used in [11]. By dividing each panel into 16 rectangular portions (8 dual rows), adding the kinetic and potential energy of 32 portions (2 symmetrical solar panels) to the kinetic energy of the central rigid portion, and using Lagrange equations, the equations of the motion of the system are obtained. In this method, the gyroscopic effect of panels is taken into account. However, due to the large number of state variables, the required time for running the simulation is longer than that in the Euler-Bernoulli model.

Elastic movement in two perpendicular directions for rod appendage can be done using the Euler-Bernoulli beam for three-dimensional analysis [12]. For this purpose, each of the two directions perpendicular to the longitudinal axis of the rod is defined by an individual function. To solve numeric problems, the mode summation procedure is used. The Euler-Bernoulli beam is assumed to offer an appropriate solution in three-dimensional motion due to the slimness of the rod because gyroscopic effect does not significantly affect the slim rods.

2. Equations of the satellite with hinged, rigid panels

The model is comprised of two symmetric, hinged, rigid panels, a torsional spring with *k* stiffness, and a torsional damper with a damping rate of *c* placed at the hinge. It is shown in Fig. 1.

2.1 Reference frames

The reference frame B $(\vec{b}_1,\vec{b}_2,\vec{b}_3)$ is connected to the satellite body, and its origin is located at the center of mass of the system. The system is free to rotate with respect to the inertial fixed frame I $(\vec{e}_1,\vec{e}_2,\vec{e}_3)$. Each panel is hinged to the body at point $C_i (i=1,2)$, which is defined by vector $\vec{r}_{Ci}$ in reference frame B. Frame P_i $(\vec{e}_{li},\vec{e}_{ni},\vec{e}_{ri})$ is attached to the *ith* panel, and its origin is positioned on the hinge axis. Unit vector $\vec{e}_{ri}$ is aligned with the hinge axis. Vector $\vec{e}_{li}$ is aligned with the direction of the longitudinal axis of the panel from the hinge toward the center of mass of the panel. The third vector is perpendicular to the two previous vectors ($\vec{e}_{ni}=\vec{e}_{ri}\times\vec{e}_{li}$). Column matrix $\mathbf{e}_{ri}$ defines the direction of vector $\vec{e}_{ri}$ in frame B:

$$\vec{e}_{ri}=e_{ri1}\vec{b}_1+e_{ri2}\vec{b}_2+e_{ri3}\vec{b}_3= [\vec{b}_1 \quad \vec{b}_2 \quad \vec{b}_3]\begin{bmatrix} e_{ri1} \\ e_{ri2} \\ e_{ri3} \end{bmatrix}=[\vec{b}_1 \quad \vec{b}_2 \quad \vec{b}_3]\mathbf{e}_{ri} \tag{1}$$

Matrix $\mathbf{E}_{pi}=[\mathbf{e}_{li} \quad \mathbf{e}_{ni} \quad \mathbf{e}_{ri}]$ describes the direction of the *ith* panel in body frame B. Vector $\mathbf{r}_{Ci}$ and matrix $\mathbf{E}_{pi}$ are arbitrary, so the position and the direction of solar panels relative to frame B are arbitrary. The center of mass of each panel is located at a distance d from the hinge. θ_i is the rotation angle of each panel about the hinge axis relative to its equilibrium position. Defining $\mathbf{e}_{l0i}$ and $\mathbf{e}_{n0i}$ as the primary directions for $\theta_i=0$, $\mathbf{e}_{li}$ and $\mathbf{e}_{ni}$ for other angles are obtained from the following equations:

$$\mathbf{e}_{li}=+\mathbf{e}_{l0i}\cos\theta_i+\mathbf{e}_{n0i}\sin\theta_i \tag{2a}$$

$$\mathbf{e}_{ni}=-\mathbf{e}_{l0i}\sin\theta_i+\mathbf{e}_{n0i}\cos\theta_i \tag{2b}$$

The time derivative of $\mathbf{e}_{li}$ and $\mathbf{e}_{ni}$ is as follows:

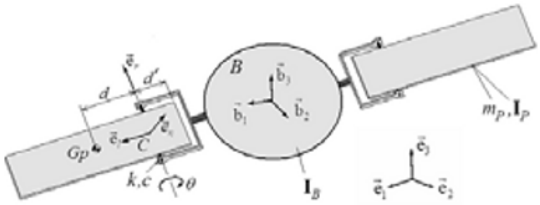

Fig. 1. Satellite with two symmetrical, hinged, rigid panels.

$$\dot{\mathbf{e}}_{li} = \dot{\theta}_i \mathbf{e}_{ni} \qquad \dot{\mathbf{e}}_{ni} = -\dot{\theta}_i \mathbf{e}_{li} \tag{3}$$

2.2 Kane's equation

Kane's method is utilized to derive the equations of motion of the satellite (body and hinged panels). To describe the motion of the system thoroughly, N generalized speeds (quasi-velocities), u_k, are required. For the satellite central body and two hinged panels, five quasi-velocities can be chosen as follows:

$$\boldsymbol{\omega} = \boldsymbol{\omega}_B = u_1 \mathbf{b}_1 + u_2 \mathbf{b}_2 + u_3 \mathbf{b}_3 \tag{4}$$

$$u_{i+3} = \dot{\theta}_i \qquad i = 1,2 \tag{5}$$

The first three quasi-velocities are the components of the absolute angular velocity of the body in frame B, and two other quasi-velocities are the angular velocities of the panels relative to the central body. Kane's equation for a set of M rigid bodies, defined by N quasi-velocities, is given in Eq. (6) [13, 14]:

$$U_k^* = U_k \qquad k = 1,2,...,N \tag{6}$$

In the above equation, U_k^*, the *kth* generalized inertia force, is obtained from the following:

$$U_k^* = \sum_{j=1}^{M} \left(m_j \mathbf{a}_{Gj}^T \mathbf{v}_{Gj}^k + \dot{\mathbf{h}}_{Gj}^T \boldsymbol{\omega}_j^k \right) \qquad k = 1,2,...,N \tag{7}$$

where m_j is the mass of the *jth* body, and $\mathbf{a}_{Gj}$ and $\dot{\mathbf{h}}_{Gj}$, are the absolute acceleration of the mass center and time derivative of the absolute angular momentum of the *jth* body about its mass center, respectively. The superscript T represents the transpose of vectors and the substitutes for the vector inner product. Partial velocities $\mathbf{v}_{Gj}^k$ and $\boldsymbol{\omega}_j^k$ are calculated by

$$\begin{aligned} \mathbf{v}_{Gj}^k &= \partial \mathbf{v}_{Gj} / \partial u_k \\ \boldsymbol{\omega}_j^k &= \partial \boldsymbol{\omega}_j / \partial u_k \end{aligned} \qquad k = 1,2,...,N \tag{8}$$

The kth generalized effective force U_k is obtained from

$$U_k = \sum_{j=1}^{M} \left(\mathbf{F}_j^T \mathbf{v}_{Gj}^k + \mathbf{M}_{Gj}^T \boldsymbol{\omega}_j^k \right) \qquad k = 1,2,...,N \tag{9}$$

In the above equation, $\mathbf{F}_j$ is the result of all effective forces applied to the *j*th body through its mass center, and $\mathbf{M}_{Gj}$ is the resultant of all effective moments applied to the *j*th body on its mass center. In this equation, only the effective forces and moments that can do work are taken into account.

2.3 Kinematics of motion and quasi-velocities

The angular velocity vector of each panel in frame B is obtained from

$$\boldsymbol{\omega}_{Pi} = \boldsymbol{\omega} + \dot{\theta}_i \mathbf{e}_{ri} \tag{10}$$

The velocity and acceleration of the mass center of each panel in frame B are respectively given by the following:

$$\mathbf{v}_{GPi} = \mathbf{v}_{Ci} + \boldsymbol{\omega}^{\times} \mathbf{r}_{GPi/Ci} + \mathbf{v}_{GPi/Ci}^{rel} = \boldsymbol{\omega}^{\times} \mathbf{r}_{GPi} + d\dot{\theta}_i \mathbf{e}_{ni} \tag{11}$$

$$\mathbf{a}_{GPi} = \dot{\boldsymbol{\omega}}^{\times} \mathbf{r}_{GPi} + \boldsymbol{\omega}^{\times} \boldsymbol{\omega}^{\times} \mathbf{r}_{GPi} + 2d\dot{\theta}_i \boldsymbol{\omega}^{\times} \mathbf{e}_{ni} - d\dot{\theta}_i^2 \mathbf{e}_{li} + d\ddot{\theta}_i^2 \mathbf{e}_{ni} \tag{12}$$

where $\mathbf{r}_{GPi} = \mathbf{r}_{Ci} + d\mathbf{e}_{li}$, and the matrix $\boldsymbol{\omega}^{\times}$ is a matrix operator for a cross-product. In previous sections, all nonzero partial velocities are obtained using the following formulas:

$$\begin{aligned} \mathbf{v}_{GPi}^1 &= r_{GPi2} \mathbf{b}_3 - r_{GPi3} \mathbf{b}_2 \\ \mathbf{v}_{GPi}^2 &= r_{GPi3} \mathbf{b}_1 - r_{GPi1} \mathbf{b}_3 \qquad i = 1,2 \\ \mathbf{v}_{GPi}^3 &= r_{GPi1} \mathbf{b}_2 - r_{GPi2} \mathbf{b}_1 \end{aligned} \tag{13}$$

$$\mathbf{v}_{GPi}^k = d\mathbf{e}_{ni} \qquad k = 4,5 \qquad i = 1,2 \tag{14}$$

$$\boldsymbol{\omega}_B^k = \mathbf{b}_k \qquad k = 1,2,3 \tag{15}$$

$$\boldsymbol{\omega}_{Pi}^k = \mathbf{b}_k \qquad k = 1,2,3 \qquad i = 1,2 \tag{16}$$

$$\boldsymbol{\omega}_{Pi}^k = \mathbf{e}_{ri} \qquad k = 4,5 \qquad i = 1,2 \tag{17}$$

2.4 Generalized forces

The effective forces and moments are:

$$\mathbf{M}_{GB} = \mathbf{M}_C + (k\theta_1 + c\dot{\theta}_1)\mathbf{e}_{r1} + (k\theta_2 + c\dot{\theta}_2)\mathbf{e}_{r2} \tag{18}$$

$$\begin{aligned} \mathbf{M}_{GP1} &= -(k\theta_1 + c\dot{\theta}_1)\mathbf{e}_{r1} \\ \mathbf{M}_{GP2} &= -(k\theta_2 + c\dot{\theta}_2)\mathbf{e}_{r2} \end{aligned} \tag{19}$$

where $\mathbf{M}_C$ is the control moment vector applied to the satellite body. The hinged forces and hinged momentums do not carry out work in the system. Finally, generalized forces are obtained as

$$\begin{aligned} U_1 &= M_{C1} = \mathbf{M}_C^T \mathbf{b}_1 \\ U_2 &= M_{C2} = \mathbf{M}_C^T \mathbf{b}_2 \\ U_3 &= M_{C3} = \mathbf{M}_C^T \mathbf{b}_3 \end{aligned} \tag{20}$$

$$\begin{aligned} U_4 &= -k\theta_1 - c\dot{\theta}_1 \\ U_5 &= -k\theta_2 - c\dot{\theta}_2 \end{aligned} \tag{21}$$

2.5 Equations of motion

As indicated by Eq. (14), the component of acceleration of

the mass center of the panel along the direction of $\mathbf{e}_{ni}$ is required, and after simplification, the following is obtained:

$$a_{GPni} = (r_{GPli}\mathbf{e}_{ri}^T - r_{Cri}\mathbf{e}_{li}^T)\dot{\boldsymbol{\omega}} + \omega_{ri}(\omega_{ni}r_{Cri} - \omega_{ri}r_{Cni}) + \omega_{li}(\omega_{ni}r_{GPli} - \omega_{li}r_{Cni}) + d\ddot{\theta}_i \quad (22)$$

where $r_{GPli} = \mathbf{e}_{li}^T\mathbf{r}_{Ci} + d$, $\omega_{ri} = \mathbf{e}_{ri}^T\boldsymbol{\omega}$, $r_{Cri} = \mathbf{e}_{ri}^T\mathbf{r}_{Ci}$, and the rest are also defined in the same manner. The component of time derivative of the angular momentum along $\mathbf{e}_{ri}$ is obtained by using the following formula:

$$\dot{\mathbf{h}}_{Gpri} = I_r(\mathbf{e}_{ri}^T\dot{\boldsymbol{\omega}} + \ddot{\theta}_i) + \omega_{ni}\omega_{li}(I_n - I_l) \quad (23)$$

The general inertia force, U_4^* , is obtained by using the following formula:

$$U_4^* = 0 + m_{P1}\mathbf{a}_{GP1}^T(d\mathbf{e}_{n1}) + 0 + 0 + \dot{\mathbf{h}}_{GP1}^T(\mathbf{e}_{r1}) + 0 \quad (24)$$

Using Kane's equation, the equation of motion of each panel is found to be

$$\mathbf{A}_{1i}\dot{\boldsymbol{\omega}} + B_{1i}\ddot{\theta} = C_{1i} - k\theta_i - c\dot{\theta}_i \qquad i = 1,2 \quad (25)$$

where

$$\mathbf{A}_{1i} = I_r\mathbf{e}_{ri}^T + m_P d(r_{GPli}\mathbf{e}_{ri}^T - r_{Cri}\mathbf{e}_{li}^T) \quad (26)$$

$$B_{1i} = I_r + m_P d^2 \quad (27)$$

$$C_{1i} = m_P d[r_{Cni}(\omega_{ri}^2 + \omega_{li}^2) - \omega_{ni}(\omega_{ri}r_{Cri} + \omega_{li}r_{GPli})] - \omega_{li}\omega_{ni}(I_n - I_l) \quad (28)$$

In the above equations, m_p is the mass of each panel. In a similar way, the equations of motion of the satellite body are obtained using the following formula:

$$\mathbf{A}_2\dot{\boldsymbol{\omega}} + \mathbf{B}_2\ddot{\theta} = \mathbf{C}_2 \quad (29)$$

where

$$\mathbf{A}_2 = \mathbf{I}_{GB} + 2\mathbf{E}_P\mathbf{I}_{GP}\mathbf{E}_P^T - 2m_P\mathbf{r}_P^{\times}\mathbf{r}_P^{\times} \quad (30)$$

$$\mathbf{B}_2 = 2m_P d\mathbf{r}_P^{\times}\mathbf{e}_n + 2I_r\mathbf{e}_r \quad (31)$$

$$\mathbf{C}_2 = \mathbf{M}_C - 2\dot{\theta}[(I_l - I_n)(\omega_l\mathbf{e}_n + \omega_n\mathbf{e}_l) + 2m_P d\mathbf{r}_P^{\times}\boldsymbol{\omega}^{\times}\mathbf{e}_n] + 2m_P\mathbf{r}_P^{\times}(d\dot{\theta}^2\mathbf{e}_l - \boldsymbol{\omega}^{\times}\boldsymbol{\omega}^{\times}\mathbf{r}_P) - \boldsymbol{\omega}^{\times}[(\mathbf{I}_{GB} + 2\mathbf{I}_{GP})\omega + 2I_r\dot{\theta}\mathbf{e}_r] \quad (32)$$

3. Satellite model with hinged, rigid panels in ADAMS

In Fig. 2, the satellite model with hinged panels in ADAMS software is shown. This model is created to evaluate the equations found in the previous section. The model consists of a central rigid body as the satellite body and two rigid panels connected to the central body via a revolute joint. In each joint, a torsional spring and a torsional damper have been added between two adjacent parts.

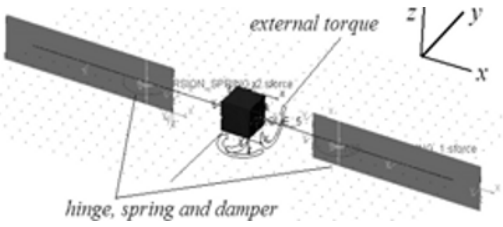

Fig. 2. Satellite model with hinged, rigid panels in ADAMS.

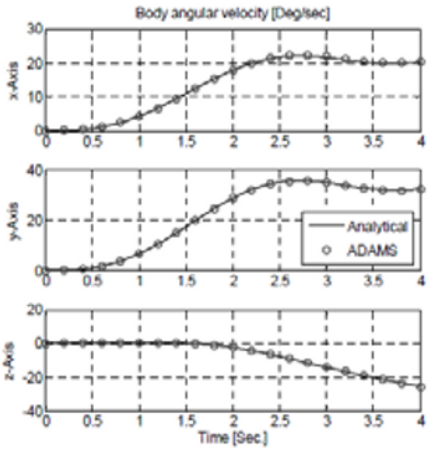

Fig. 3. Body angular velocity for the satellite model with two symmetric hinged panel.

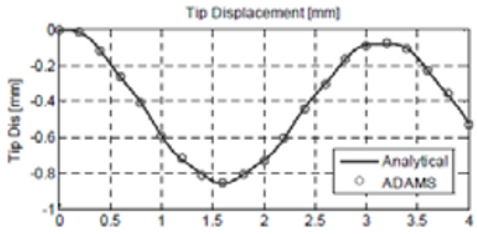

Fig. 4. Panel tip displacement for hinged panels.

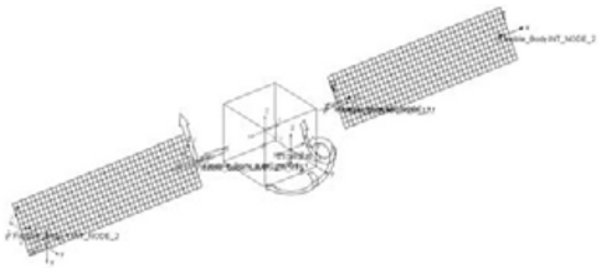

Fig. 5. Satellite model with flexible panels in ADAMS.

To facilitate comparison, the initial longitudinal and perpendicular directions of the panels are assumed in the x and y axes relative to the body frame respectively.

To compare the analytical model and the model built in ADAMS software, the same input has been given to the two models:

$$\mathbf{M}_e = (1 - \cos(2t)) \times [1 \quad 100 \quad 5]^T N \cdot mm \quad (33)$$

A small amount has been chosen for the torque component around the x axis because the inertia of the satellite around this axis is small. To show the gyroscopic effect, the torque component around the z axis is supposed to be small as well. Figure 3 illustrates the components of angular velocity of the satellite during 4 seconds. The solid lines represent the results of the numerical solution of equations discussed in the previous section, which are obtained from MATLAB software. The circles show the results of the satellite model in ADAMD software. The tip displacement of each solar panel is also shown in Fig. 4 for comparison.

As shown, the results are consistent with one another. The ADAMS model is built in a graphical environment and simply by defining mass, inertia, geometrical dimensions, rate of springs, and other parameters without the need to determine analytical equations. In comparison, to obtain the results from MATLAB software, all the equations derived in the previous section need to be solved using one of the numerical solving methods of this software. The absolute consistency between the results of these two methods, considering their fundamental differences, confirms the accuracy of the analytical equations derived in the previous section. Based on the results mentioned earlier, there is no difference between the hinged, rigid panels in ADAMS and the analytical model of the hinged, rigid panels in MATLAB. Therefore, hereafter, both are dubbed as hinged, rigid -panel models.

4. Flexible satellite model using the Euler-Bernoulli beam

In this method, the position of each point of the flexible panel center line relative to its non-deformed position is determined as a function of time and its distance from the fixed end of the beam. Using the mode summation procedure, the vibration behavior in different frequencies is simulated. For deriving the equations of motions of solar panels by the Euler-Bernoulli beam model, the Lagrange equation can be used as follows:

$$\frac{d}{dt}\left(\frac{\partial L}{\partial \boldsymbol{\omega}}\right)+\boldsymbol{\omega}^{\times}\left(\frac{\partial L}{\partial \boldsymbol{\omega}}\right)=\mathbf{M}_C \tag{34}$$

$$\frac{d}{dt}\left(\frac{\partial L}{\partial \dot{w}}\right)-\frac{\partial L}{\partial w}+\frac{\partial}{\partial x}\left(\frac{\partial L}{\partial w'}\right)-\frac{\partial^2}{\partial x^2}\left(\frac{\partial L}{\partial w''}\right)=0 \tag{35}$$

In the above equations, $L=T-V$ is the Lagrangian of the system, and $w=w(x,t)$ is the lateral displacement of the beam. Using the separation of variable method, a continuous function $w(x,t)$ can be written in the form of the product of functions $v(t)$ and $\psi(x)$:

$$w(x,t)=\sum_{q}^{N}\psi_q(x)v_q(t) \tag{36}$$

Function $\psi_q(x)$ can be written in the following form:

$$\psi_q(x)=\cosh(\lambda_q x)-\cos(\lambda_q x)-R_q(\sinh(\lambda_q x)-\sin(\lambda_q x)) \tag{37}$$

where R_q is calculated from the following equation:

$$R_q=\frac{\cosh(\lambda_q L_P)+\cos(\lambda_q L_P)}{\sinh(\lambda_q L_P)+\sin(\lambda_q L_P)} \tag{38}$$

The eigenvalues λ_q are calculated based on the characteristic equation given below and obtained from Eq. (37) using the boundary conditions (clamped at the fixed end and free at the other end):

$$\cos\lambda L_P\cosh\lambda L_P=-1 \tag{39}$$

Ref. [15] has thoroughly presented the equations of motion of a satellite by the Euler-Bernoulli beam in three-dimensional motion.

5. Satellite model with flexible panels in ADAMS

The flexible satellite model in ADAMS software contains one central rigid body and two flexible panels fixed to the central rigid body at one edge as shown in Fig. 5. The dynamic model is built based on modes summation procedure and considering the entire possible modes for a panel, such as bending, torsion, and so on. Each panel is divided into 400 rectangle-shaped elements. The first six modes of each panel are shown in Fig. 6. The flexible panel model in ADAMS, considering different mode shapes, represents the dynamic behavior of a system that is better than other models.

6. Frequency response comparison of the models

In Fig. 7, the transfer function of the satellite with flexible panels as the ratio of the magnitude of the body angular velocity about the z axis to the magnitude of the input torque about this axis is shown in dB unit with a broken line. The system input is a torque around the z axis, which has been applied to the center of mass of the rigid body of the satellite. As can be seen, at the frequency of $2.56Hz$, the ratio of altitude of the body angular velocity to the altitude of the input torque becomes minimum. By increasing the frequency, the altitude of angular velocity increases. At $6.11Hz$, the altitude reaches a maximum.

Assuming that the density of the solar panels does not change, along their length, the center of mass of each panel is placed at its geometrical center.

While the panel is considered as a hinged, rigid panel, the optimum position of the hinge is not the edge of the panel because changing the stiffness of the torsional spring cannot match both the first and second frequencies with the relative frequencies of the equivalent satellite with flexible solar panels. As a result, the position of the hinge relative to the panel edge is considered as the second parameter for matching natural frequencies.

In Fig. 8, the effect of the hinge position and stiffness of the torsional spring on the two natural frequencies of satellite with

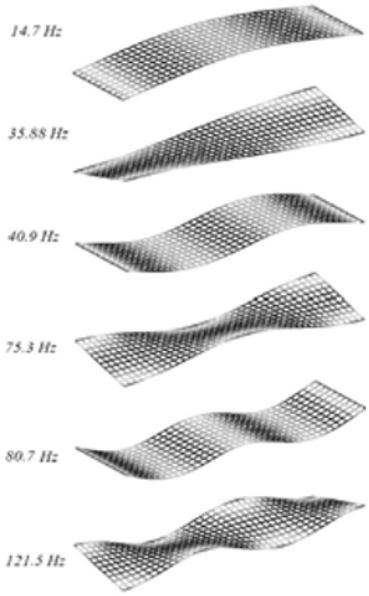

Fig. 6. The first six natural modes of each solar panel.

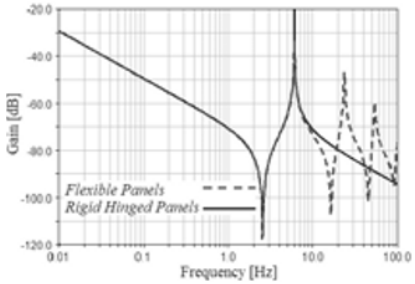

Fig. 7. Transfer function of angular velocity of the satellite body.

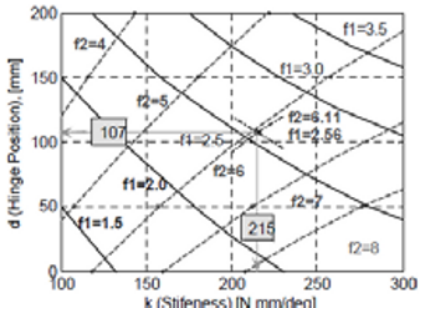

Fig. 8. Effect of hinge position and spring stiffness on the first (solid lines) and second (broken lines) frequencies.

rigid panels is shown. Constant frequency curves are shown with solid lines for the first frequency and with broken lines for the second frequency. The increase in stiffness of torsional springs causes an increase in both natural frequencies of the system, while an increase in the distance of the hinge from the panel tip causes an increase in the first frequency and a decrease in the second frequency. The appropriate position and stiffness for obtaining $2.56Hz$ and $6.11Hz$ frequencies are specified from the intersection of the curves related to these values. The value obtained for the position of the hinge is $107mm$, and for torsion stiffness, it is $215N \cdot mm/\deg$.

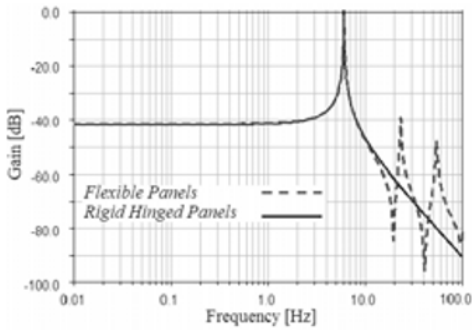

Fig. 9. Transfer function of the displacement of solar panels' tip.

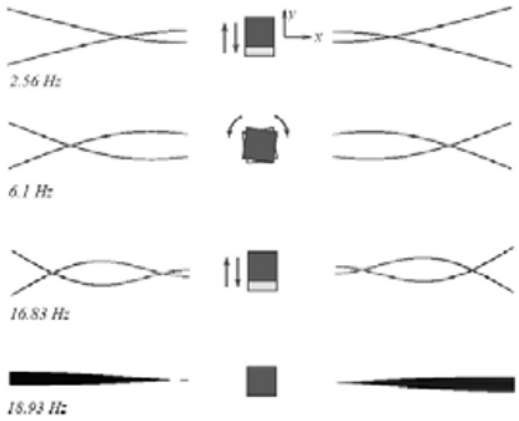

Fig. 10. First natural modes of the satellite with flexible panels.

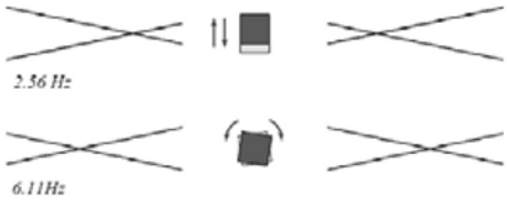

Fig. 11. Natural mode shapes of the satellite with two symmetric hinged, rigid panel.

In Fig. 7, the frequency transfer function for the satellite with hinged, rigid panels for the hinge position of $107mm$ and torsion stiffness of $215N \cdot mm/\deg$ is shown with a continuous line. As shown in this figure, there is a good correspondence between the two models for frequencies less than $8Hz$. Beyond this frequency, however, the results of the hinged, rigid -panel model and the flexible-panel model deviate from each other.

In Fig. 9, the frequency transfer function as the proportion of the altitude of panel tip displacement to the altitude of the input torque around the z axis in "dB" is shown in a broken line for the satellite with flexible panels and in a solid line for the satellite with hinged, rigid panels. As can be seen, at the frequency of $6Hz$, the altitude of panel displacement is at a maximum, and there is a good correspondence between the two models up to $10Hz$.

The first four natural mode shapes of the satellite with flexible panels are illustrated in Fig. 10. In each mode shape, for a

better observation of nodal points, the image of the satellite and its panels are in two ends of the vibration amplitude (with 180° phase apart). At the first natural frequency ($2.56Hz$), the mode shape of the panel is bending, and one node is generated in each panel. In this state, the satellite body has linear motion along the y axis and moves in the opposite direction of two-panel motion. At a frequency of $6.11Hz$, the mode shape is bending, one node is generated in the panel, and the satellite body has an angular motion on the z axis.

In Fig. 11, the natural mode shapes of the satellite with hinged, rigid panels are illustrated. As shown, at the first frequency ($2.56Hz$), the satellite motion is exactly the same as the first mode of the satellite with flexible panels. The satellite motion at the second natural frequency ($6.11Hz$) is also exactly similar to the second mode of the satellite with flexible panels, and the position of nodes is almost similar as well. Regarding the curvature in the mode shapes of flexible panels, a slight difference in the position of nodes is expected.

The satellite with rigid panels does not include the higher natural frequencies of the satellite with a flexible panel. The third frequency of flexible panels ($16.83Hz$) is also associated to the bending mode, which is not observed in the frequency response of the hinged, rigid -panel model. The fourth mode ($22.33Hz$) is associated with the torsion of panels around the x axis.

Dividing each panel into several parts and considering the simple joint, torsional spring, and torsional damper between two adjacent parts, a more comprehensive model of the rigid panel is created to improve hinged, rigid -panel model behavior in higher frequencies. However, ignoring the torsion of panels and dividing solar panels into several hinged parts are useful if the highest frequency obtained for bending does not skip, roughly speaking, two or more of the torsional mode frequencies.

7. Comparison of models' behavior in the time domain

In this section, the same input torques are applied to the three models, namely, the hinged, rigid -panel model, the Euler-Bernoulli beam model, and the flexible-panel model (ADAMS), to compare the behavior of these different models in the time domain. The input is chosen so that they highlight the major differences between these models. As the first input, the torque is applied to the body just around the z axis:

$$\mathbf{M}_C = (1-\cos(10\times 2\pi\times t))\times[0 \quad 0 \quad 10]^T N\cdot mm \qquad (40)$$

This input has the most influence in the bending of the panels. The second input resembles the first one, but the frequency grows up to 30Hz:

$$\mathbf{M}_C = (1-\cos(30\times 2\pi\times t))\times[0 \quad 0 \quad 10]^T N\cdot mm \qquad (41)$$

As the third input, the three-dimensional torque applied to the body, unlike the two mentioned input, does not have any component on the z axis:

$$\mathbf{M}_C = (1-\cos(2t))\times[5 \quad 200 \quad 0]^T N\cdot mm \qquad (42)$$

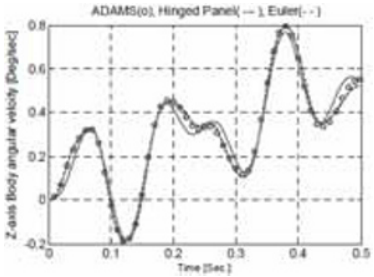

Fig. 12. z component of the angular velocity of the body to the first input.

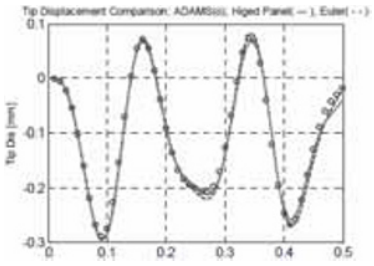

Fig. 13. Displacement of the panel tip to the first input.

The components of body angular velocity and the displacement of the panel tip due to the application of the first input to the three satellite models are illustrated in Figs. 12 and 13, respectively. The response of the Euler-Bernoulli beam model is obtained using the first three mode shapes. The other two components of the body angular velocity are zero.

While the input frequency increases from $10Hz$ to $30Hz$, the results of the Euler-Bernoulli beam model (broken line) continue to match the results of the full model in the ADAMS software (circles). However, there is a considerable difference between the results of the body angular velocity of the hinged-panels model (solid lines) and the full model in ADAMS (Figs. 14 and 15). Regarding Figs. 7 and 9, this difference is predictable at a frequency of $30Hz$. Considering Figs. 7 and 9, with frequencies over $10Hz$, the difference between the results of the flexible-panels model and the hinged-panel model are expected to increase. If only the first mode of the Euler-Bernoulli model (dash-dot curves) is used, a big variation in the results of angular velocity will be generated, and a behavior similar to that seen in the hinged panel will be attained.

In Fig. 16, the portion of displacement of the panel tip due to each of the first three modes of the Euler-Bernoulli model is shown. The first modes have more effect on the displacement of the panel tip. However, by adding each mode to the summation of previous modes, the result will be more accurate.

Finally, the third input torque is applied to the satellite. Due to the gyroscopic effect and with the generating components of angular velocity around the x and y axes, the panels will rotate around the z axis. In Fig. 17, the components of angular velocity are shown. Fig. 18 illustrates the displacement of the panel tip resulting from the application of the three-dimensional torque to the satellite.

As shown, the results from the satellite with flexible panels

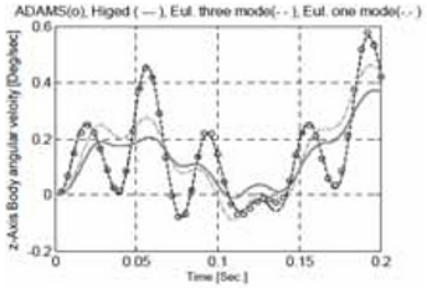

Fig. 14. z component of the angular velocity of the body to the second input.

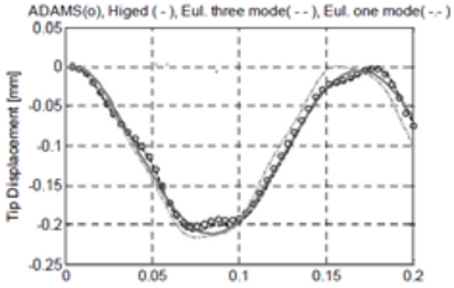

Fig. 15. Displacement of the panel tip to the second input.

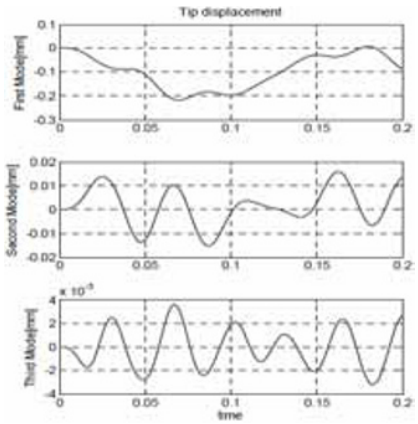

Fig. 16. Portion of each mode in the displacement of the panels' tip for the second input.

in ADAMS (circles) and in the hinged-panel models (solid lines) are consistent with each other. However, the results of the Euler-Bernoulli beam model do not match those of the two above-mentioned models.

8. Conclusion

A simple and accurate model for a flexible satellite is proposed and compared with the Euler-Bernoulli model of a flexible satellite generally used in the literature. A comprehensive model of the flexible satellite considering solar panels as flexible, finite element panels is provided in an ADAMS environment as reference when comparing the two models. Numerical simulations show identical results for the three models in planar (two-dimensional) motion.

The Euler-Bernoulli model is clarified to be inappropriate for studying the three-dimensional motion of the flexible satellite, especially the study of panel vibration, due to missing

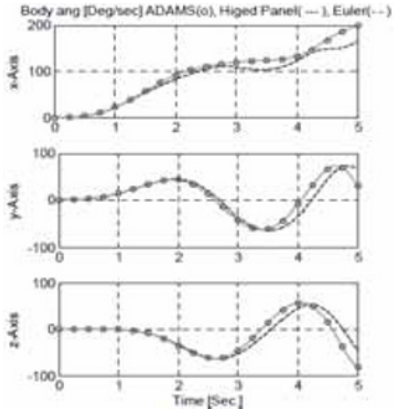

Fig. 17. Components of body angular velocity to the third input.

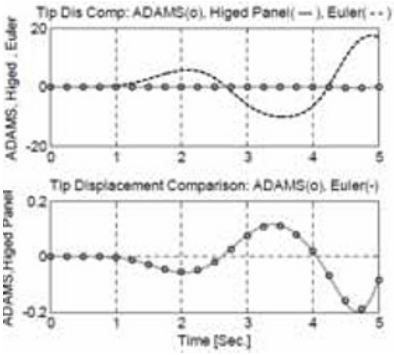

Fig. 18. Displacement of the panels' tip to the third input.

information on the gyroscopic effect in this model. On the other hand, the proposed hinged, rigid -panel model provides an accurate model of the flexible satellite both in two- and three-dimensional typical maneuvers, which produce low-frequency vibrations in the solar panels. Finally, a multi-hinged panel model is suggested as an accurate model for studying two- and three-dimensional maneuvers at higher frequencies, as well as lower frequencies if the appropriate position for the hinges and the correct stiffness for torsional springs between adjacent panel pieces are chosen.

Acknowledgment

This work has been supported partially by the Iran Telecommunication Research Center (ITRC).

Nomenclature

$\mathbf{a}$	:	Acceleration vector
$\mathbf{b}$, $\vec{b}$	:	Unit vectors of the body frame
c	:	Damping rate of each torsional damper
d	:	Distance from the mass center of the panel to the hinge
$\mathbf{e}$, $\vec{e}$	:	Unit vectors of other frames in the body frame
$\mathbf{E}$	:	Transfer matrix of the panel frame to the satellite body
$\mathbf{F}$	:	Resultant of applied forces to the body
$\mathbf{h}$	:	Absolute angular momentum vector
$\dot{\mathbf{h}}$	:	Time derivative of the absolute angular momentum
I , $\mathbf{I}$	:	Inertia moment vector

k : Stiffness rate of each torsional spring
L : Lagrangian
L_P : Length of each solar panel
$\mathbf{M}$: Resultant moments on the body center of mass
m : Mass
N : Number of generalized speeds (quasi-velocities)
$\mathbf{r}$, $\vec{r}$: Position vector
T : Kinetic energy of the entire system
t : Time
$\mathbf{v}_G^k$: Partial linear velocity of the kth center of mass
U_k : kth generalized effective force
U_k^* : kth generalized inertia force
u_k : kth quasi-velocity
V : Potential energy of the entire system
w : Lateral displacement of the Euler-Bernoulli beam
x : Distance of a point on the beam to its support
$\mathsf{I}, \mathsf{B}, \mathsf{P}$: Inertia frame, body frame, panel frame
λ_q : Eigenvalue of the qth mode shape
v : Modal displacement
ψ : Mode shape function
θ : Rotation angle of the panel on the hinge axis
ω , $\boldsymbol{\omega}$: Angular velocity
$\boldsymbol{\omega}^k$: kth partial angular velocity

References

[1] Y. Zeng, A. D. Araujo and S. N. Singh, Output feedback variable structure adaptive control of flexible spacecraft, *Acta Astronautica,* 44 (1) (1999) 11-22.

[2] H. Bang, Y. Cho and H. Lee, Slewing maneuver control of flexible spacecraft by output feedback, *Acta Astronautica,* 55 (2004) 903-916.

[3] Q. Hu and G. Ma, Variable structure control and active vibration suppression of flexible spacecraft during attitude maneuver, *Aerospace Science and Technology*, 9 (2005) 307-317.

[4] Q. Hu and Y. Liu, A hybrid scheme of feed-forward/feed-back control for vibration suppression of flexible spacecraft with on-of actuators during attitude maneuver, *International Journal of Information technology,* 11 (12) (2005) 95-107.

[5] B. N. Agrawal, R. S. Mcclelland and G. Song,, Attitude control of flexible spacecraft using pulse-width pulse-frequency modulation thrusters, *Space Technology*, 17 (1) (1997) 15-34.

[6] G. Song and B. N. Agrawal, Vibration suppression of flexible spacecraft during attitude control, *Acta Astronautica*, 49 (2) (2001) 73-83.

[7] Y. Chida, H. Soga, Y. Yamaguchi, T. Kida, I. Yamaguchi and T. Sekiguchi, On-orbit attitude control experiment using ETS-VI by H_∞ control and two-degree-of-freedom control, *Control Engineering Practice*, 6 (1998) 1109-1116.

[8] D. Gorinevsky and G. Vukovich, Control of flexible spacecraft using nonlinear approximation of input shape dependence on reorientation maneuver parameters, *Control Engineering Practice*, 5 (12) (1997) 1661-1671.

[9] J. Zheng, S. P. Banks and H. Alleyne, Optimal attitude control of three-axis stabilized flexible spacecraft, *Acta Astronautica*, 56 (2005) 519-528.

[10] H. Bang, C. Ha and J. H. Kim, Flexible Spacecraft attitude maneuver by application of sliding mode control, *Acta Astronautica*, 57 (2005) 841-850.

[11] S. Parman and H. Koguchi, Controlling the attitude maneuvers of flexible spacecraft by using time-optimal/fuel-efficient shaped inputs, *Journal of Sound and Vibration*, 221 (4) (1999) 545-565.

[12] A. D. Meglio and A. Ercolifinzi, Minimum time control of flexible spacecraft by Hamilton's principle, *Meccanica*, 32 (1997) 555-565.

[13] T. R. Kane, P. W. Likins and D. A. Levinson, *Spacecraft Dynamics*, McGraw-Hill, (1981).

[14] H. Baruh, *Analytical dynamics*, McGraw-Hill, Singapore, (1999).

[15] K. A. Ford and C. D. Hall, Reorienations of spacecraft using momentum exchange devices, Ph.D. Dissertation, *air force inst of tech. Wright-Patterson AFB* (1997).

Shahram Shahriari received his B.S. and M.S. degrees in Mechanical Engineering from the Sharif University of Technology in Iran in 1993 and 1998, respectively. He is currently a Ph.D. candidate in Tarbiat Modares University, Iran. His main research interests are in the area of robust control, multi-body dynamics, vehicle engineering, and satellite attitude control and dynamics.

Shahram Azadi received his BS and MS in Mechanical Engineering from the Sharif University of Technology, Iran in 1989 and 1992, respectively. He then received his PhD from the Amir-Kabir University of Technology in 1999. Currently, he is an Assistant Professor at the School of Mechanical Engineering at K.N. Toosi University of Technology in Tehran, Iran. His research interests include dynamics, control, and automotive engineering.

Majid Moghaddam received his B.Sc. degree in Mechanical Engineering in 1988 from the Sharif University of Technology, Iran, his M.Eng. degree in Mechanical Engineering in 1993 from McGill University, Canada, and his Ph.D. degree in Mechanical Engineering in 1996 from the University of Toronto, Canada. He is Professor of mechanical engineering at Tarbiat Modares University, Tehran, Iran. His current research, which focuses on applied robotics and robust H∞ control, is concerned with haptic robotics, rehabilitation robotics, inspection robotics, and rough terrain mobile robot design. He is a member of the Administrative Committee of the Mechatronics Society of Iran. He has served as co-chair for many national /international conferences in Iran.